Title

Sound Measurement in Patient-Specific 3D Printed Bench Models of Venous Pulsatile Tinnitus.

Journal

Otology & neurotology : official publication of the American Otological Society, American Neurotology Society [and] European Academy of Otology and Neurotology, 41(1)

ISSN

1531-7129

Authors

Valluru, Keerthi
Parkhill, James
Gautam, Ayushi
et al.

Publication Date

2020

DOI

10.1097/mao.0000000000002452

Peer reviewed

HHS Public Access

Author manuscript

Otol Neurotol. Author manuscript; available in PMC 2021 January 01.

Published in final edited form as:

Otol Neurotol. 2020 January ; 41(1): e7–e14. doi:10.1097/MAO.0000000000002452.

Sound measurement in patient-specific 3D printed bench models of venous pulsatile tinnitus

Keerthi Valluru, MS[1], **James Parkhill, BS**[1], **Ayushi Gautam, BS**[1], **Henrik Haraldsson, PhD**[1], **Evan Kao, PhD**[1], **Joseph Leach, MD, PhD**[1], **Alexandra Wright, MD**[1], **Megan Ballweber, BS**[1], **Karl Meisel, MD**[2], **David Saloner, PhD**[1], **Matthew Amans, MD**[1]

[1]UCSF Department of Radiology and Biomedical Imaging

[2]UCSF Department of Neurology

Abstract

Hypothesis: We hypothesize patient-specific flow models to be an adequate *in vitro* surrogate to allow for characterization of Pulsatile Tinnitus that affects 3–5 million Americans.

Background: Pulsatile tinnitus (PT), rhythmic sounds without an extracorporeal source that patients appreciate, can be caused by aberrant blood flow in large cerebral veins near the cochlea. In order to investigate the sound production mechanism, we created 3D printed flow models based on patient-specific cerebral venous anatomies.

Methods: Magnetic resonance angiography datasets from two patients with PT were used to generate patient-specific 3D printed flow models. A flow circuit connecting the patient-specific models to a pulsatile, continuous flow pump simulating cardiac cycle was created. Sound recordings were made along the surface of the models using an electronic stethoscope. Peak-to-rms amplitude, and area under the power spectral density (PSD) curve values were computed to evaluate the sound measurements. Wilcoxon rank sum test was used to statistically determine the differences in measurements between the patient-specific models.

Results: In patient-1, the recordings (peak-to-rms) from the internal jugular vein stenosis of baseline model (4.29±1.26 for 146 samples) were significantly louder ($p<0.001$) than that of the altered model (3.29±0.96 for 143 samples). In patient-2, the sound measured at the transverse sinus stenosis in the pre-lumbar puncture model (4.84±1.11 for 148 samples) was significantly louder ($p<0.0001$) than that of the post-lumbar puncture model (3.14±0.87 for 135 samples).

Conclusions: The models are able to generate sounds very similar to those appreciated by patients and examiners in the cases of objective PT.

Introduction

Tinnitus is the auditory perception of sound in the absence of an external source that affects millions of Americans [1]. Patients' lives can be severely adversely impacted by tinnitus, and

Corresponding author: Matthew Amans MD, MSc, Assistant Professor of Radiology and Biomedical Imaging, Divisions of Neurointerventional Radiology and Neuroradiology, University of California, San Francisco, 505 Parnassus Ave, Room L349, San Francisco, CA 94143, Matthew.Amans@ucsf.edu, Telephone: 415-353-1863.

it is not uncommon for patients to suffer from insomnia, depression, or even have suicidal ideations because of their tinnitus [2–9]. A subset of tinnitus is rhythmic and termed pulsatile tinnitus (PT). PT accounts for up to 10% of tinnitus cases [10–12]. Some causes of PT are associated with a very high risk of intracranial hemorrhage, stroke, or blindness. However, even the more “benign” causes of PT have a very high association with debilitating comorbid psychiatric disease. Some causes of PT can be treated. In our experience, treating an underlying cause of PT not only alleviates the risks of hemorrhage, stroke, or blindness, but can also mitigate the co-morbid psychiatric disease. As such, identifying and treating causes of PT can be beneficial for patients.

PT may be related to abnormal flow in vascular structures near the cochlea, and is often pulse-synchronous[1,11]. The vascular structures with aberrant flow can be either venous or arterial. Approximately 40% of PT etiologies are venous, approximately 35% are arterial, and in nearly 25% of cases the cause of PT is never identified [13]. The most commonly implicated venous structures are the transverse sinus, sigmoid sinus, and internal jugular vein (SSIJ) [1]. Decreasing the flow of blood through the venous sinuses near the cochlea by manual compression of the ipsilateral internal jugular vein (IJV) decreases these patients’ PT; high-flow states such as in contralateral IJV compression, exercise, or during pregnancy increases symptoms [13,14]. Treatment of the particular anatomic abnormality in the SSIJ can resolve PT[14–19]; however, sometimes the treatment can carry significant risks of intracranial hemorrhage or ischemic stroke. In order to develop new treatments, an appropriate bench-top model needs to be developed.

Reduced costs, increased access, and improved awareness of 3D printing software and hardware has led to steep increases in the application of 3D printed patient-specific anatomic models to a variety of applications from patient-specific implant design, intraoperative reference models, planning of catheter-based interventions, and other procedural planning and training [20]. The aim of this study is to apply 3D printing techniques to generate patient-specific in vitro flow models of the SSIJ. These models are used to further understand the mechanism of sound production in venous causes of pulsatile tinnitus and ultimately to provide a testing mechanism for future device development to treat the condition.

Methods

We prospectively performed MR analysis on adult patients with suspected venous etiology of pulsatile tinnitus using a study protocol approved by our Institutional Review Board (IRB). All patients provided written informed consent to participate in this study. From the high-resolution MR image data, patient-specific flow models were created using 3D printing techniques. A flow-circuit was created using these models and sound was measured and recorded using a Bluetooth stethoscope.

PT was suspected to be of venous etiology if patients described a low-pitch, pulse synchronous PT that improved with ipsilateral neck compression, and potential arterial (or other) etiologies (such as carotid atherosclerosis, fibromuscular dysplasia, tumor, or dural arteriovenous fistula) had not been identified on prior imaging studies. All patients had the MRI and MRA that included brain MRI with fat-saturated post contrast sequences, time

resolved contrast enhanced MRA (CE-MRA) of the neck through the circle of Willis, and post contrast spoiled gradient (SPGR) MRI to evaluate venous sinus anatomy.

Imaging

In this study, the approach used to obtain high contrast images of the vascular anatomy is an adaptation of CE-MRA methods described in prior manuscripts[21–24]. CE-MRA was performed on a 1.5T scanner (Philips Healthcare, Andover, Massachusetts). A 3D TWIST timing run with a 2cc Gd bolus was used to determine the venous phase of contrast opacification as the point when the contrast first appears in the distal transverse sinus. The full CE-MRA study was then performed with a 20cc injection of Gd-based contrast agent at 2cc/sec with an acquisition time of 35 secs. Images had 0.7 mm isotropic resolution covering a field of view of 280 mm x 180 mm with an 84 mm thick slab. Image acquisition used an elliptic centric k-space ordering with the center of k-space synchronized to the venous phase as determined from the timing run. The major adjustment in this study was the use of a large volume acquisition to provide broad coverage of the venous anatomy. The resultant acquisition time was substantially longer than in conventional CE-MRA studies which are run in the arterial phase and require shorter acquisitions to avoid venous contamination.

Patient-specific flow models—A surface representation of the SSIJ from the affected side was segmented from the CE-MRA volumetric dataset using Vascular Modeling Toolkit (Orobix, Bergamo, Italy), processed with ParaView (Clifton Park, NY), and exported as a Standard Tessellation Language (STL) mesh file. Using Autodesk Fusion 360 (San Rafael, CA), the mesh file was modified by adding 6.35 mm diameter flow extensions at the inlet (the entrance to the transverse/sigmoid sinus) and the outlet (exit from the internal jugular vein) to allow connections via tubing to a rotary pump. The STL file was imported onto a 3D printer (3ZMax^2, Solidscape, Inc., Merrimack, NH) and the luminal anatomy was printed in wax with a slice thickness of 0.0381 mm. The wax lumen was embedded in a degassed solution of silicone encapsulant (Sylgard® 184, Dow Corning, Midland, MI) which was cured for 48 hours. The inner wax lumen was then melted out of the silicone and removed from the models by heating at 120°C to create a durable and rigid patient-specific SSIJ flow model (Figure 1).

Four total flow models were created from two patients. Patient one has a high-riding jugular bulb and stenosis of the internal jugular vein at the level of the first cervical vertebrae (Figure 1A). An additional modified flow model for this patient was created by computationally relieving the stenosis (Figure 1B). Two models are of a patient with idiopathic intracranial hypertension and a transverse sinus stenosis (Figure 1C). This patient underwent a therapeutic and diagnostic lumbar puncture (LP). After lowering her intracranial pressure (ICP) via LP, her symptoms resolved, and an additional MRA was performed. An additional flow model was generated from the post-LP MRA (when the patient reported resolution of PT) (Figure 1D).

Flow circuit—A flow circuit connecting the patient-specific models to a pulsatile, continuous flow pump using clear plastic tubing was created. Pulsatile-continuous flow was established by triggering a programmable servo drive pump (BLuAC5-Si, Applied Motion

Products, Watsonville, CA) with a repetitive signal simulating the cardiac cycle (60 bpm). After calibrating the flow rate, the pump was tuned to generate water flow at a rate of 9cc/s. In each patient-specific flow circuit, the flow models representing the discrete conditions mentioned above were connected in series and positioned side by side on a sound insulating platform with the model orientation approximating the supine position. Serial connection of the models allowed for sound measurements in both the baseline and altered models to be obtained using the exact same flow rate.

Sound recording

To ensure reproducible positioning of the stethoscope, markings were made on the surface of each of the models where sound would be measured. Sound recordings (20 – 2000 Hz, 15 secs long, 24X amplification) were made using a Bluetooth-compatible electronic stethoscope (3M Littmann 3200, St. Paul, MN) in a noise-free environment. To facilitate sound transmission, ultrasound gel was applied between the hands-free stethoscope and the model during the experiments. To assess the reproducibility of sound generation ten separate pairs of recordings were made in both the baseline and altered models. The pump was turned off and back on again between each set of recordings. The sound recordings instantaneously transmitted via Bluetooth to a PC allowed real time visualization of sound signals.

Sound processing

The signals were processed and analyzed in MATLAB R2018b (Mathworks, Natick, MA). Nonlinear baseline trends and ultralow frequency noise were removed from the recordings by fitting a low order polynomial and subtracting it, and then applying a high pass filter with a cutoff frequency of 80 Hz. As a measure of sound intensity of the generated pulsatile sound, peak-to-rms amplitude values were calculated for each pulse. Frequency analysis was performed to yield power spectral density, normalized to the loudest signal within the flow circuit (PSD = $10*\log_{10}[P_1/P_0]$ dB/Hz with P_1 = power of the signal being evaluated, and P_0 = power of the loudest signal). Area under the curve (AUC) values were then determined to estimate the cumulative distribution of power as a function of frequency. Wilcoxon rank sum test was used to determine differences in peak-to-rms amplitude and the AUC values between the baseline and altered models.

Results and Discussion

3D printed benchtop flow models of patient specific venous anatomy were created, reliably and reproducibly generating sounds very similar to venous PT (Audio file SDC3_baseline.wav and Audio file SDC4_altered.wav in Supplemental Digital Content correspond to the sound recordings obtained from patient one at the internal jugular vein in baseline model and altered model respectively. Audio file SDC5_preLP.wav and Audio file SDC6_postLP.wav in Supplemental Digital Content represent the sound recordings collected from patient two at the transverse sinus region in pre-LP model and post-LP model respectively).

In patient one, the recordings from the baseline model were louder than from the altered model, $p<0.001$ (Figures 2A, 2B, 3A, and 3B). Ten separate 15 s long sound recordings at

the IJV of baseline and altered models yielded minimal intra-model variation (mean ± standard deviation) in peak-to-rms amplitude values (4.29 ± 1.26 for 146 samples in baseline model, 3.29 ± 0.96 for 143 samples in altered model; Figure SDC1A in Supplemental Digital Content). Qualitatively, the PSD plots comparing the baseline and altered model show a dramatic increase, by an order of magnitude, in the frequencies around and below 600Hz in the baseline model compared to the altered model (Figures 4A and 4B). This suggests the main power of PT sounds is in the lower frequency range between 80 and 600 Hz. The mean AUC of ten PSD vs. frequency plots for baseline model was significantly greater than with the altered model −172413.09 ± 14438.30 vs. −188966.66 ± 9436.34, respectively (p=0.0140) (Figure SDC2A in Supplemental Digital Content).

In patient two, lowering the ICP via LP resulted in expansion of the venous sinus stenosis similar to what other authors have documented[25–28]. The sound was loudest at the transverse sinus stenosis in the pre-LP model (Figure 2C) which rapidly decayed with stethoscope positioning further away along the vein. Similar to the patient's clinical report of complete resolution of PT after her LP, the post-LP flow model produced nearly no residual measurable sound at a similar spot in the transverse sinus (Figure 2D). Ten separate sound recordings at the transverse sinus of pre-LP and post-LP models yielded minimal intra-model variation in mean peak-to-rms amplitude values (4.84 ± 1.11 for 148 samples in pre-LP model, 3.14 ± 0.87 for 135 samples in post-LP model; Figure SDC1B in Supplemental Digital Content), with pre-LP model being significantly louder (p<0.0001) than the post-LP model (Figures 3C and 3D). The PSD plots showed that the frequencies up to 600 Hz in the pre-LP model have a PSD higher than −60 dB, an order of magnitude higher than the PSD of the same frequencies in the post-LP model similar to the results obtained from patient one (Figures 4C and 4D). The mean AUC of ten PSD vs. frequency plots for pre-LP model was −159955.30 ± 11451.71, significantly larger (p=0.0003) than the mean AUC of −188260.39 ± 6362.26 yielded from ten PSD plots for post-LP model (Figure SDC2B in Supplemental Digital Content).

While others have used 3D printing for evaluation of sinus pericranii and for pre-operative planning[29,30] and even to evaluate dehiscence of the sigmoid sinus cortical plate in pulsatile tinnitus patients[31], ours are the first 3D printed models of the dural venous sinuses to show not only sound generation but also the effects of lumbar puncture in patients with IIH. The main limitation of this work is the limited number of subjects. However, this is a novel application of evolving 3D printing techniques that has resulted in successful creation of *in vitro* patient-specific models for venous PT that generate sounds very similar to those reported by patients. We acknowledge that the data presented here is by no means inclusive of the comprehensive list of venous etiologies that could cause PT. In patient one, our hypothesis was that the IJV stenosis in combination with high riding bulb was the main source of PT. The sound recordings from the computationally modified IJV supported this hypothesis as the sound intensity was substantially decreased by the removal of the stenotic segment. However, there remained a significant sound production in the altered model emanating from the jugular bulb. Our data from patient two suggests that the sound resolution after LP that correlated with the patient's relief in symptoms is a result of improvement in the transverse sinus stenosis.

The rigid walls and use of water as our fluid are additional limitations of our model as these do not match *in vivo* conditions. The 3D printed silicone walls are rigid and much thicker than *in vivo*. While these limitations are not physiologically accurate, the development of sound similar to what patients experience suggests that the flow patterns, rather than wall motion, are primarily responsible for PT generation in the venous sinuses. In these initial experiments we also used water, a Newtonian fluid whose viscosity is independent of the flow velocity. To simulate blood that is fundamentally non-Newtonian in nature, future work will use a glycerol-water mixture, as has been reported by other authors [32,33]. Materials for each model costs less than USD 100 to manufacture. Approximately 3 days is needed to develop a model from the MRI data. Much of this time is spent in curing the materials. Our 3D printing technique resulted in the generation of accurate patient-specific vascular models. We believe that these models could be valuable not only in identifying the anatomical location of sound generation but could also aid in determining the flow characteristics responsible for sound generation. Identifying the responsible fluid dynamics could lead to development of novel treatments.

Conclusions

This technical report presents the first *in vitro* patient-specific flow model for venous causes of PT based on CE-MRA images. The models are able to generate sounds very similar to those appreciated by patients and examiners in the cases of objective PT with high reliability. Our results suggest patient-specific flow models may be an appropriate *in vitro* surrogate for investigations of venous causes of PT.

Supplementary Material

Refer to Web version on PubMed Central for supplementary material.

Acknowledgments

Grant support:

This project was supported by the National Center for Advancing Translational Sciences, National Institutes of Health, through UCSF-CTSI Grant Number B27552C. In addition, this research reported in this publication was supported by the National Institutes of Health under award number R21 DC016087–01A1. Its contents are solely the responsibility of the authors and do not necessarily represent the official views of the NIH.

References

1. Krishnan A, Mattox DE, Fountain AJ, Hudgins PA. CT arteriography and venography in pulsatile tinnitus: preliminary results. AJNR Am J Neuroradiol 2006;27(8):1635–1638. [PubMed: 16971601]
2. Belli S, Belli H, Bahcebasi T, Ozcetin A, Alpay E, Ertem U. Assessment of psychopathological aspects and psychiatric comorbidities in patients affected by tinnitus. Eur Arch Otorhinolaryngol 2008;265(3):279–285. [PubMed: 17999075]
3. Weidt S, Delsignore A, Meyer M, et al. Which tinnitus-related characteristics affect current health-related quality of life and depression? A cross-sectional cohort study. Psychiatry Res 2016.
4. Xu Y, Yao J, Zhang Z, Wang W. Association between sleep quality and psychiatric disorders in patients with subjective tinnitus in China. Eur Arch Otorhinolaryngol 2016.
5. Pridmore S, Walter G, Friedland P. Tinnitus and suicide: recent cases on the public record give cause for reconsideration. Otolaryngol Head Neck Surg 2012;147(2):193–195. [PubMed: 22535918]

6. Jacques D, Nozeret Y, Zdanowicz N, Reynaert C, Garin P, Gilain C. Tinnitus and psychiatric comorbidities in liaison psychiatry analysis of three years in an audiophonology centre. Psychiatr Danub 2013;25 Suppl 2:S102–104. [PubMed: 23995155]
7. Zirke N, Seydel C, Arsoy D, et al. Analysis of mental disorders in tinnitus patients performed with Composite International Diagnostic Interview. Qual Life Res 2013;22(8):2095–2104. [PubMed: 23292277]
8. Seo JH, Kang JM, Hwang SH, Han KD, Joo YH. Relationship between Tinnitus and Suicidal Behavior in Korean Men and Women: a Cross-sectional Study. Clin Otolaryngol 2015.
9. Seydel C, Haupt H, Szczepek AJ, Hartmann A, Rose M, Mazurek B. Three years later: report on the state of well-being of patients with chronic tinnitus who underwent modified tinnitus retraining therapy. Audiol Neurootol 2015;20(1):26–38. [PubMed: 25413891]
10. Liyanage SH, Singh A, Savundra P, Kalan A. Pulsatile tinnitus. J Laryngol Otol 2006;120(2):93–97. [PubMed: 16359136]
11. Madani G, Connor SE. Imaging in pulsatile tinnitus. Clin Radiol 2009;64(3):319–328. [PubMed: 19185662]
12. Harvey RS, Hertzano R, Kelman SE, Eisenman DJ. Pulse-synchronous tinnitus and sigmoid sinus wall anomalies: descriptive epidemiology and the idiopathic intracranial hypertension patient population. Otol Neurotol 2014;35(1):7–15. [PubMed: 24270723]
13. Mattox DE, Hudgins P. Algorithm for evaluation of pulsatile tinnitus. Acta Otolaryngol 2008;128(4):427–431. [PubMed: 18368578]
14. Otto KJ, Hudgins PA, Abdelkafy W, Mattox DE. Sigmoid sinus diverticulum: a new surgical approach to the correction of pulsatile tinnitus. Otol Neurotol 2007;28(1):48–53. [PubMed: 17195746]
15. Houdart E, Chapot R, Merland JJ. Aneurysm of a dural sigmoid sinus: a novel vascular cause of pulsatile tinnitus. Ann Neurol 2000;48(4):669–671. [PubMed: 11026453]
16. Eisenman DJ. Sinus wall reconstruction for sigmoid sinus diverticulum and dehiscence: a standardized surgical procedure for a range of radiographic findings. Otol Neurotol 2011;32(7):1116–1119. [PubMed: 21799456]
17. Liu Z, Chen C, Wang Z, et al. Sigmoid sinus diverticulum and pulsatile tinnitus: analysis of CT scans from 15 cases. Acta Radiol 2013.
18. Santa Maria PL. Sigmoid sinus dehiscence resurfacing as treatment for pulsatile tinnitus. J Laryngol Otol 2013:1–3.
19. Amans MRSC, Dowd CF, Higashida RT, Hetts SW, Cooke DL, Narvid J, Halbach VV. Resolution of Pulsatile Tinnitus after Coil Embolization of Sigmoid Sinus Diverticulum. Austin J Cerebrovasc Dis & Stroke 2014;1(2):1010.
20. George E, Liacouras P, Rybicki FJ, Mitsouras D. Measuring and Establishing the Accuracy and Reproducibility of 3D Printed Medical Models. Radiographics 2017;37(5):1424–1450. [PubMed: 28800287]
21. Kao E, Kefayati S, Amans MR, et al. Flow patterns in the jugular veins of pulsatile tinnitus patients. J Biomech 2016.
22. Kefayati S, Amans M, Faraji F, et al. The manifestation of vortical and secondary flow in the cerebral venous outflow tract: An in vivo MR velocimetry study. J Biomech 2017;50:180–187. [PubMed: 27894675]
23. Acevedo-Bolton G, Amans MR, Kefayati S, Halbach V, Saloner D. Four dimensional magnetic resonance velocimetry for complex flow in the jugular vein. Quantitative Imaging in Medicine and Surgery 2015;5(4):635–637. [PubMed: 26435930]
24. Amans M, Haraldsson H, Kao E, et al. MR Venous Flow in Sigmoid Sinus Diverticulum. American Journal of Neuroradiology 2018(in press).
25. Scoffings DJ, Pickard JD, Higgins JN. Resolution of transverse sinus stenoses immediately after CSF withdrawal in idiopathic intracranial hypertension. J Neurol Neurosurg Psychiatry 2007;78(8):911–912. [PubMed: 17635988]
26. King JO, Mitchell PJ, Thomson KR, Tress BM. Manometry combined with cervical puncture in idiopathic intracranial hypertension. Neurology 2002;58(1):26–30. [PubMed: 11781401]

27. Baryshnik DB, Farb RI. Changes in the appearance of venous sinuses after treatment of disordered intracranial pressure. Neurology 2004;62(8):1445–1446. [PubMed: 15111701]

28. Onder H, Gocmen R, Gursoy-Ozdemir Y. Reversible transverse sinus collapse in a patient with idiopathic intracranial hypertension. BMJ Case Rep 2015;2015.

29. Simonin A, Martinerie S, Levivier M, Daniel RT. Three-dimensional printing of a sinus pericranii model: technical note. Childs Nerv Syst 2017;33(3):499–502. [PubMed: 28247114]

30. Ryan JR, Almefty KK, Nakaji P, Frakes DH. Cerebral Aneurysm Clipping Surgery Simulation Using Patient-Specific 3D Printing and Silicone Casting. World Neurosurg 2016;88:175–181. [PubMed: 26805698]

31. Tian S, Fan X, Wang Y, Liu Z, Wang L. An in vitro experimental study on the relationship between pulsatile tinnitus and the dehiscence/thinness of sigmoid sinus cortical plate. J Biomech 2019;84:197–203. [PubMed: 30665710]

32. Hochareon P, Manning KB, Fontaine AA, Deutsch S, Tarbell JM. Diaphragm motion affects flow patterns in an artificial heart. Artif Organs 2003;27(12):1102–1109. [PubMed: 14678424]

33. Samavat H, Evans JA. An ideal blood mimicking fluid for doppler ultrasound phantoms. J Med Phys 2006;31(4):275–278. [PubMed: 21206644]

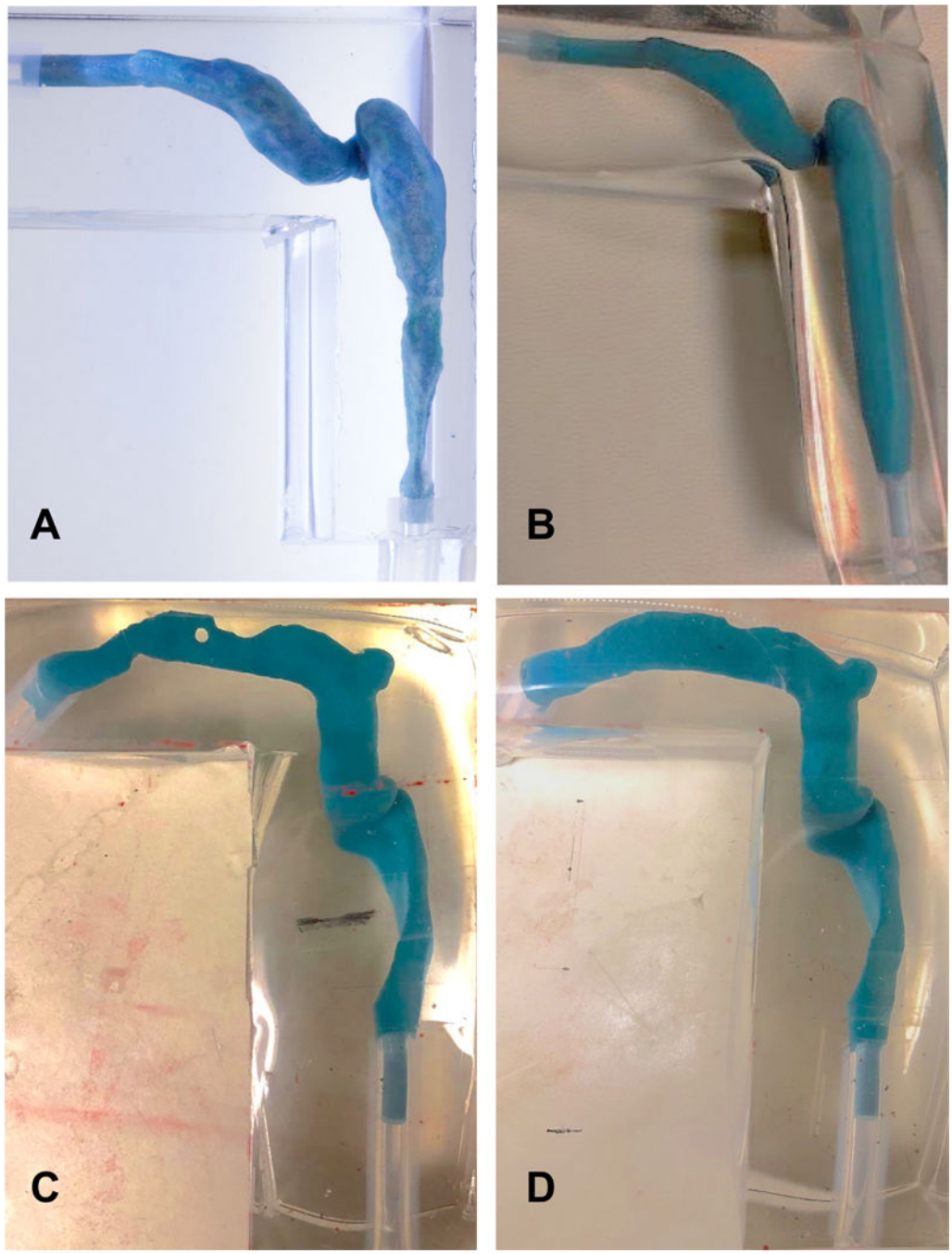

Figure 1.

A) 3D printed venous segment of patient one showing native cerebral venous sinus and jugular vein derived from the CE-MRA dataset, and **B)** The venous anatomy was reprinted after computationally modifying the internal jugular vein to remove the stenosis across C1 transverse process. 3D printed venous segment of patient two showing transverse sinus, sigmoid sinus, and internal jugular vein derived from CE-MRA acquired: **C)** before lumbar puncture, and **D)** after lumbar puncture. The drainage of cerebrospinal fluid led to a decrease in ICP and dilation of the transverse sinus, notably alleviating the patient's PT.

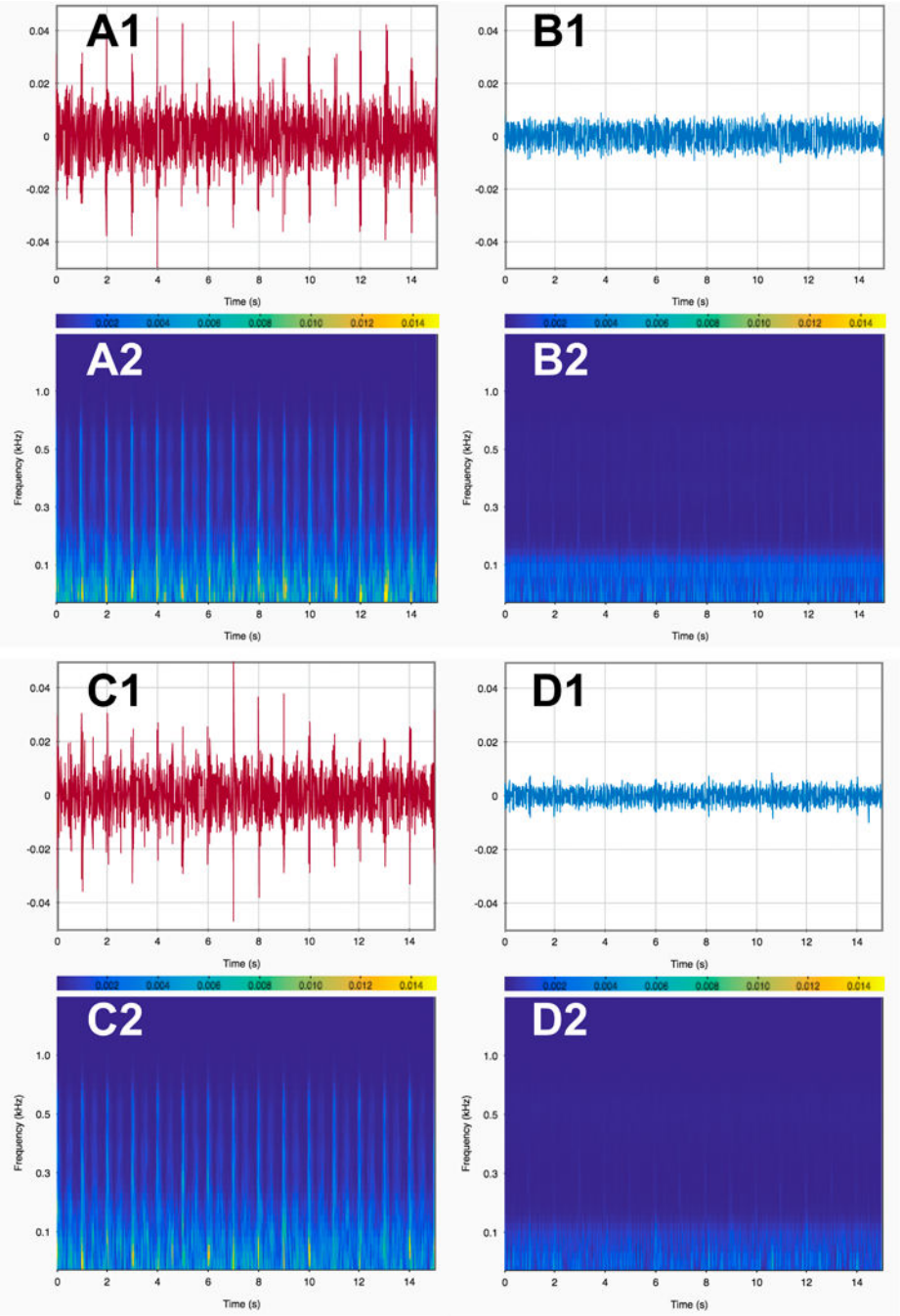

Figure 2.

A1) Sound intensity signals from the internal jugular vein (IJV) region of the baseline IJV model (figure 1 A) measured over a duration of 15 seconds and the corresponding frequency vs time scalogram (**A2)**. **(B1)** Sound intensity signals from the altered IJV model (figure 1 B) and the corresponding scalogram (**B2)**. (**C1)** Sound intensity signals from the transverse sinus region in pre-lumbar puncture (preLP) model measured over a duration of 15 seconds and the corresponding scalogram (**C2)**. (**D1)** Sound intensity signals from the post-LP model, and corresponding scalogram (**D2)**. The measured sounds in A1, A2, C1, and C2

were pulse-synchronous to the pump cycle triggered at 60 beats per minute demonstrated the characteristic crescendo-decrescendo nature of venous pulsatile tinnitus.

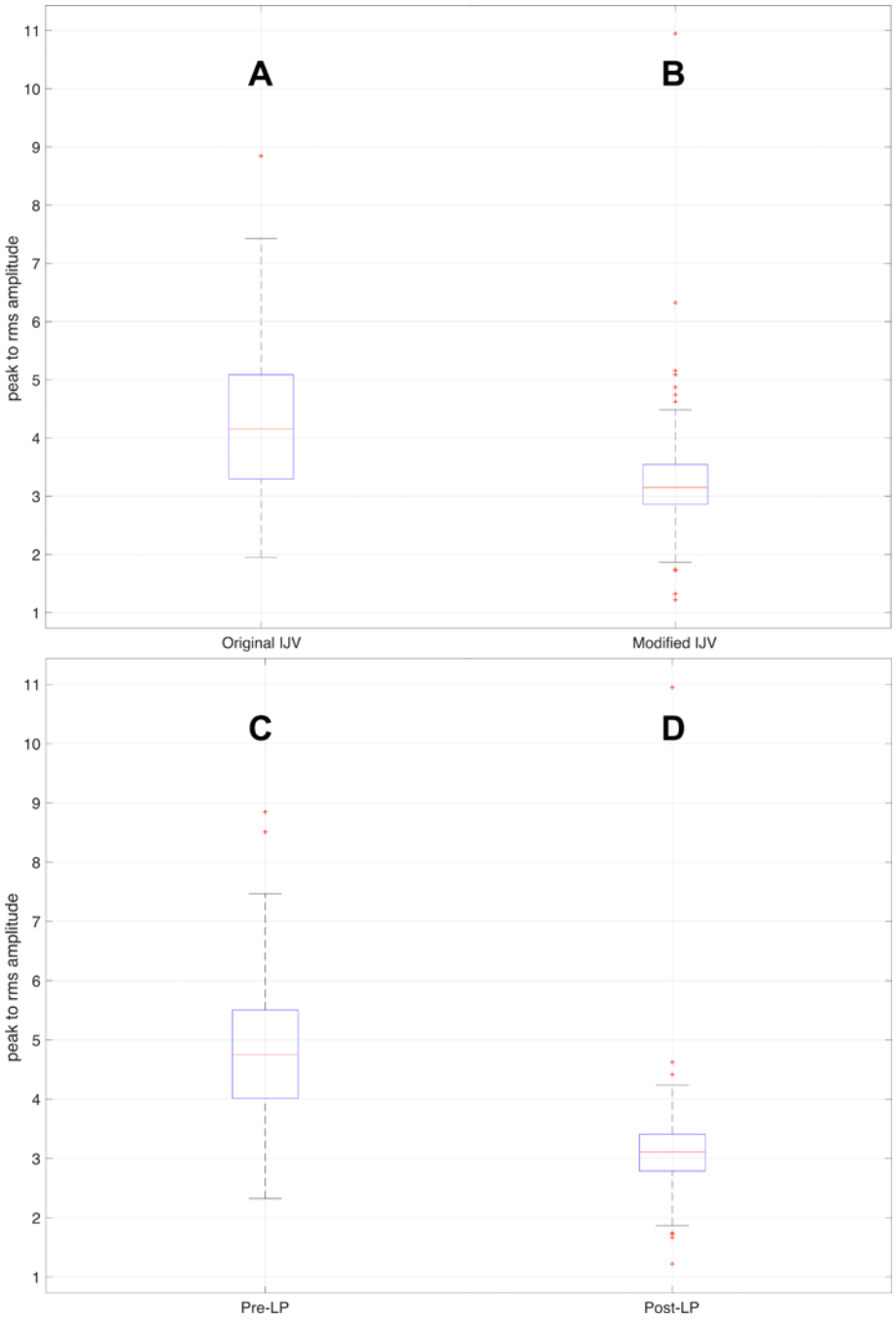

Figure 3.

(A) Analysis of peak-to-rms amplitude values as a measurement of sound intensity recorded from baseline patient one model (seen in figure 1A), and peak-to-rms amplitude values from **(B)** altered model (seen in figure 1B). The baseline patient one model was louder than the altered model ($p<0.0001$). (C) Analysis of peak-to-RMS amplitude values recorded over the transverse sinus stenosis in the model from patient 2 (seen in figure 1C), and peak-to-RMS values from the post-LP model measured in the same location over the transverse sinus (D) (seen in figure 1D). Corresponding to the patient's reported improvement in symptoms after

LP, the pre-LP model was significantly louder than the post-LP model ($p<0.0001$). The box and whiskers plots show median (central line) peak-to-rms amplitude value with the bottom and top edges of the box indicating the 25th and 75th percentiles, respectively. The whiskers represent the most extreme data points not considered outliers, while the outliers are shown individually using the '+' symbol.

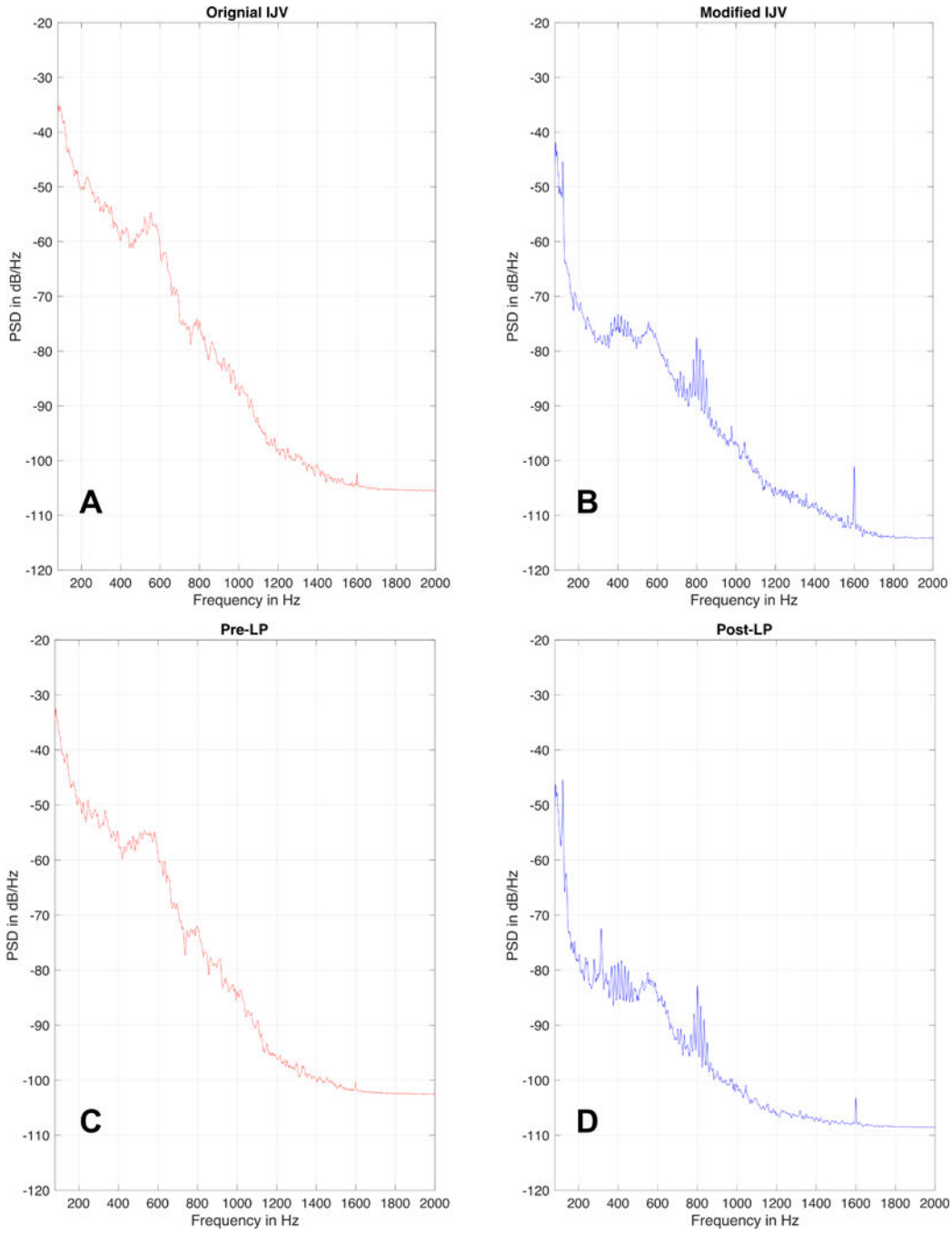

Figure 4.

Power spectral density (PSD in dB/Hz) plotted as a function of frequency (Hz) for a representative sound signal recorded at **A)** the internal jugular vein (IJV) region for the baseline IJV model of patient one, **B)** IJV region in the altered IJV model of patient one, **C)** transverse sinus location for the pre-LP model of patient two, and **D)** transverse sinus location in post-LP model of patient two. In comparing the “symptomatic” models (**A** and **C)** to the “asymptomatic” models (B and D), the PSD for frequencies up to 600 Hz was higher than −60 dB (audible volume) in the symptomatic models, but lower than −70 dB

(nearly inaudible volumes and less than half as loud as the symptomatic models) in the asymptomatic models.